Feasibility study of localised active noise control using an audio spotlight and virtual sensors

M. R. F. Kidner, C. Petersen, A. C Zander and C. H. Hansen

Active Noise and Vibration Control Group, University of Adelaide, Adelaide, Australia

ABSTRACT

Global control of sound at audio frequencies in large spaces is challenging and has been a sticking point for the development of active systems for noise control in areas such as factory floors or public spaces. Combining highly directional sound sources and virtual sensing techniques is proposed as a possible solution. Such a system would create localised zones of quiet that can follow an individual through a space. The application of a parametric array as a sound source is discussed in this paper. The parametric array creates an audible directional sound source due to the non-linear interaction of two ultrasound waves. A beamwidth of the order of a few degrees is possible at audio frequencies, however the sound levels produced are quite low. The properties of the source in regard to active control are discussed. Virtual sensing uses an array of microphones to predict the sound field at a remote point. It has been shown that active control of the sound field at a moving virtual error sensor is possible. The criteria for control performance in a 1D sound field using such a sensor are outlined. The advantages and disadvantages of the combination of these two advanced transducers for use in active noise control are discussed in this paper.

INTRODUCTION

Active control of sound can be used to create a zone of quiet (Nelson 1993), the size of which is a function of wavelength. This zone of quiet is fixed in space and is centred on the location of the error sensor. The work presented in this paper aims to overcome these limitations and create a moving zone of quiet that does not require an error sensor to be located at the point of maximum attenuation. This system has potential applications in transport and industrial environments.

The accurate sensing of the pressure field at a point remote from the location of the physical sensor has been described as virtual sensing (Munn 2003). The virtual sensor is a device that outputs a reliable estimate of the pressure at the remote point. Given this estimate of the pressure field, a zone of quiet could be produced at the remote location, thus removing the need for transducers at the point of control.

Given that zones of quiet are limited in size by the wavelength of the sound field, it is desirable to concentrate control effort on the zone of quiet alone. A highly directional sound source can be used to create a zone of quiet while limiting the areas of increased noise level outside the zone to locations within the beam. The highly directional sound source also allows for tracking of the zone of quiet and a moving virtual sensor has been developed by Petersen *et-al* (Petersen 2006).

Figure 1 illustrates the proposed concept. A listener is located within a primary field at the location shown by small dark dot. A physical sensor is placed at the location of the 'X'. The sound field at the listener is estimated from the information collected by the physical sensor using the virtual sensing algorithm. It should be noted that the listener's position relative to the physical sensor can change. The control source is highly directional and forms a narrow beam that controls the field only at the location of the virtual sensor. There is no spillover outside the beam of the secondary source. As will be discussed later, it is important that both the physical and virtual sensors are located within the secondary source beam.

The use of a parametric array or audio spotlight as the control source and the virtual sensor as the error sensor is discussed in this paper. It is shown that there are some fundamental limitations and a number of transducer design challenges to be faced.

VIRTUAL SENSING

Virtual sensing, as described above is the estimation of a field at a point remote from the physical sensor. Three approaches to the problem are briefly described here.

Forward difference prediction techniques

Kestell *et al*. (Kestell 2000) conjectured that the pressure at the virtual sensor could be estimated using forward difference prediction techniques such as a Runge Kutta approach, based on the output from a small array of microphones, (Munn 2003) and (Kestell 2000) showed experimentally that a linear estimation routine was more robust than the theoretically more accurate quadratic estimator. This method is very sensitive to the position errors and phase matching between the physical sensors (Munn 2002a 2002b).

The adaptive least mean squares estimate

The second method uses the adaptive L.M.S algorithm to estimate the weights applied to the physical sensor output so that it minimises the error between the output of physical and virtual sensor (Cazzolato 2002). This technique requires that an additional physical sensor be placed at the virtual location *a-priori* so that the adaptive algorithm can converge on the required weights. At a single frequency, the signals can be represented as rotating vectors with a given magnitude and phase. The transfer function estimate is represented by the vector that connects the signal at the real sensor to the signal that was measured at the location of the virtual sensor, see Figure 2.

It was shown (Munn 2002b) that this method outperforms the forward prediction technique in real time experiments of active noise control in a duct. The adaptive approach estimates the transfer path from the physical to virtual sensor, and so is similar to the remote microphone technique suggested by Roure and Albaraazin (Roure 1999) and Popovich

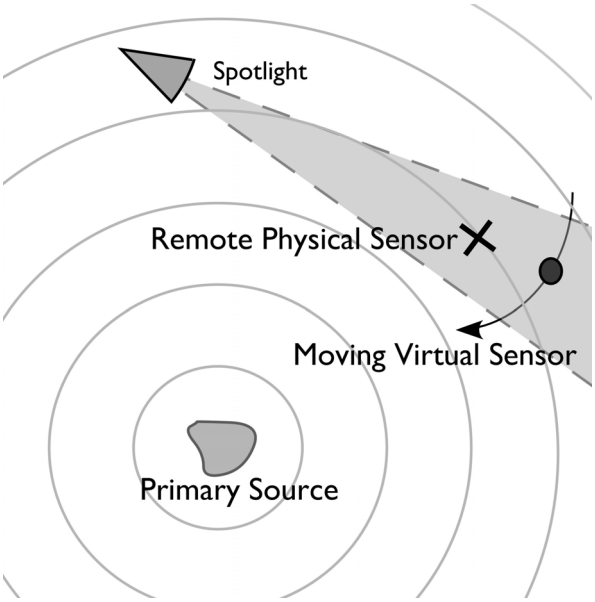

Figure 1. Illustration of the concept of a directional control source being used in combination with a virtual sensor to allow tracking of a local zone of quiet, without spillover in the rest of the field. The shaded area shows the region that is affected by the control source.

(Popovich 1997). At a single frequency both techniques are equivalent; however Cazzolato has shown (Cazzolato 2002) that only one weight/Gain is required per microphone, for broadband excitation.

It was shown (Petersen 2006a) that if the plant is lightly damped and dominated by well separated modal peaks, the average of the microphone weights estimated using white noise, converge to approximately the weights that correctly estimate the modal peaks. Therefore, implementing noise control with virtual sensors created using these average weights on the output of the physical sensors, produces reasonable estimates of the field at the location of the virtual sensor.

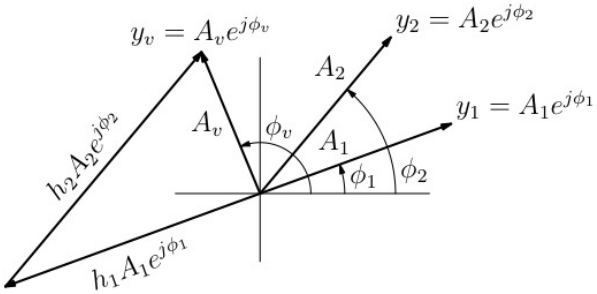

Figure 2. The vectors that represent the physical, (y_1 y_2) and virtual, (y_v) sensor output and the filter weights, (h_1 h_2), used in the adaptive L.M.S virtual microphone method.

The Remote Microphone Technique

Figure 3 shows the control diagram for the virtual sensor. It shows how the virtual microphone outputs are estimated from the *a-priori* measurement of the transfer functions between the secondary source and the virtual microphone position, $\boldsymbol{G}_{vu}$, the transfer functions from the physical to the virtual microphone position, $\boldsymbol{H}$ and the estimate of the disturbance due to the primary source, $\boldsymbol{d}$.

The algorithm works as follows;

The transfer function from the secondary source to the physical sensor is measured, and is denoted $\boldsymbol{G}_{pu}$. A physical sensor is placed at the virtual sensor location and the transfer function from the secondary source to it is measured, denoted $\boldsymbol{G}_{vu}$. With the secondary source off, the transfer function between the two sensors is measured, and denoted $\boldsymbol{H}$.

During operation, the signal that is due solely to the primary disturbance is estimated in the following way. The estimated contribution to the field at the physical sensor due to the secondary source, $\boldsymbol{uG}_{pu}$ is subtracted from the total output from the physical sensor $\boldsymbol{e}_p$. The control signal is denoted $\boldsymbol{u}$ and $\boldsymbol{G}_{pu}$ is the transfer function that was measured off-line. This results in a signal $\boldsymbol{d}$ that is due only to the primary source. The field at the virtual microphone due to the primary source can then be estimated by $\boldsymbol{Hd}$, where $\boldsymbol{H}$ is the transfer function between the physical and virtual locations in the primary field. The disturbance at the virtual microphone due to the secondary field is $\boldsymbol{uG}_{vu}$, where $\boldsymbol{G}_{vu}$ is the a-priori measurement of the transfer function from the secondary source to a physical sensor temporally located at the virtual microphone location. Therefore, the estimate of the error at the virtual microphone is the combination of the field due to the secondary source, $\boldsymbol{uG}_{vu}$, and the estimate of the field due to the primary source $\boldsymbol{dH}$, which can be written in full as

$$\mathbf{e}_v = (\mathbf{e}_p - \mathbf{u}\mathbf{G}_{pu})\mathbf{H} - \mathbf{u}\mathbf{G}_v u \tag{1}$$

This approach can also be thought of in terms of the states of the plant. The output from the physical sensor is used to estimate the states. Then these states are used, in combination with a model of the plant, to estimate the system outputs, (or pressures) at the location of the virtual sensor. The application of Kalman filter theory to this problem can yield insights into the robustness and expected performance of the technique.

The Kalman Filter Approach

Since the aim of the virtual sensing algorithm is to compute an accurate estimate of the virtual error signals, the problem of virtual sensing for active noise control can be formulated as a *linear estimation* problem (Kailath 2000). In this section, the virtual sensing problem is therefore analysed using a Kalman filtering approach. In this approach, the plant under consideration is modelled by a state-space system whose outputs are the physical and virtual error signals. This is in contrast to the remote microphone technique (Popovich 1997), (Roure 1999), where the plant is modelled by a number of FIR or IIR filters. The idea behind the Kalman filter approach taken here is that the information contained in the physical error signals can be used to compute estimates of

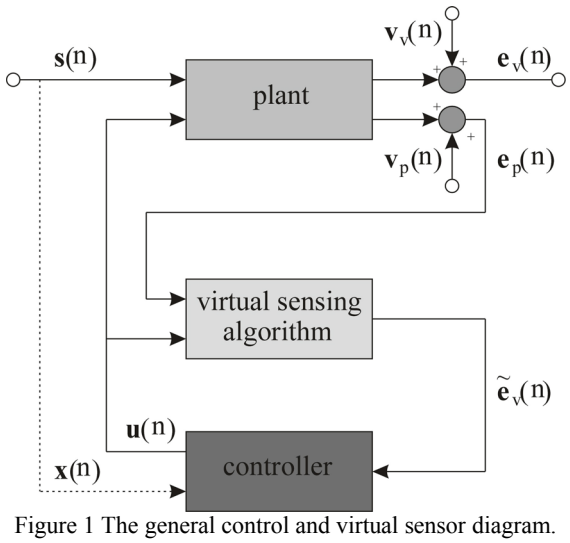

Figure 1 The general control and virtual sensor diagram.

the plant states, and the estimated plant states can be used to compute estimates of the virtual error signals.

Furthermore, measurement noise on the physical error sensors, including the ones that are placed at the virtual locations in a preliminary identification stage of the plant, can be conveniently included in the modelling of the problem. The effect of noise on the estimation performance of the virtual sensing algorithm can therefore be analysed.

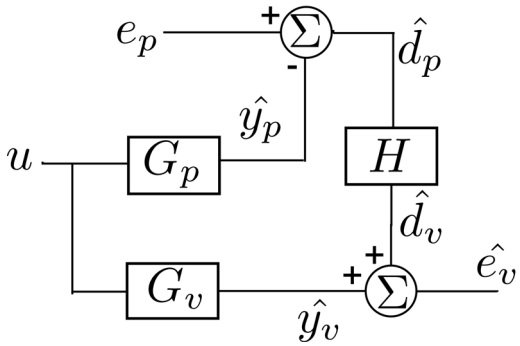

Figure 2 The virtual sensing algorithm diagram

Kalman filtering

In this section, it is assumed that physical error sensors are temporarily located at the virtual locations in a preliminary identification stage of the plant, such that the virtual error signals can be directly measured. A Kalman filter can then be formulated that computes optimal filtered estimates of the physical and virtual error signals.

Using a prediction estimator formulation, the predicted state estimates **z**(n+1|n) are computed as (Kailath 2000)

$$\tilde{\mathbf{z}}(n+1|n) = (\mathbf{A} - \mathbf{K}_s\mathbf{C})\tilde{\mathbf{z}}(n|n-1) - (\mathbf{B}_u - \mathbf{K}_s\mathbf{D})\mathbf{u}(n) + \mathbf{K}_s\mathbf{e}(n) \quad (2)$$

with $\mathbf{K}_s$ the Kalman gain matrix

given by

$$\mathbf{K}_s = \begin{bmatrix}\tilde{\mathbf{K}}_{ps} & \tilde{\mathbf{K}}_{vs}\end{bmatrix} \quad (3)$$

The matrices **C** and $\mathbf{D}_u$ are defined as

$$\mathbf{C} = \begin{bmatrix}\tilde{\mathbf{C}}_p \\ \tilde{\mathbf{C}}_v\end{bmatrix} \quad \mathbf{D} = \begin{bmatrix}\tilde{\mathbf{D}}_{pu} \\ \tilde{\mathbf{D}}_{vu}\end{bmatrix} \quad (4)$$

Discussion of virtual sensing algorithm

It has been shown that at a single frequency the Kalman filter approach and the remote microphone technique are equivalent. The performance of both is limited by the accuracy of the estimate of the virtual microphone output. This is controlled by the quality of the Kalman filter or in a physical sense, the quality of the transfer function estimate between the physical and virtual sensor and from the secondary source to the physical and virtual sensor. Petersen has shown that the control performance using a virtual microphone will always be limited by the errors in this estimate, (Petersen 2006a). In this section three scenarios in which the virtual sensor may be used in conjunction with the audio spotlight are discussed. This discussion will highlight the limitations of the method.

Figure 5 shows the three scenarios. The primary source is fixed in space relative to the error sensors. The secondary source can move. As only relative motion is important, this could be considered as the secondary source being stationary and the error sensors being moved.

Case A

Consider the situation labelled `A` in figure 5. The transfer function, ***H***, between the physical and virtual sensor in the primary field is measured *a-priori*. Due to the geometry of the primary field, this transfer function is not sensitive to horizontal changes in position of the sensors. The transfer functions, ($\boldsymbol{G}_p$ and $\boldsymbol{G}_{v)}$, from the secondary source to the physical and virtual sensors is also measured *a-priori*. The arrangement of the two sensors makes the phase of this transfer functions sensitive to small changes in horizontal position of the sensors. The transfer function $\boldsymbol{G}_\text{p}$ can be re-evaluated by an online system-id if the location of the physical sensor changes, however ***H*** and $\boldsymbol{G}_\text{v}$ are fixed.

Case B

From the discussion of the algorithm, it can be concluded that the estimate of the virtual error is sensitive to errors in ***H*** and in $\boldsymbol{G}_\text{v}$, the transfer function from the secondary source to the location of the virtual sensor (which is measured *a-priori*). When the control source is located at B, due to the narrow directivity pattern, it creates sound only at the physical sensor. The algorithm still has all the information it requires to estimate the field at the virtual sensor location. However the transfer function between the physical and virtual sensor locations due to the secondary source has a very small magnitude, as the virtual sensor is outside the beam width of the source, therefore the estimate of the field at the virtual sensor location will be very poor.

Case C

When the control source is located at C two issues arise, first, the secondary source no longer creates sound at the physical sensor. This implies that the estimate of the disturbance ***d***, will be incorrect. Also any correlation between the secondary source and the virtual error is lost, as it depends on information from the physical error, so control cannot be achieved. The second issue is that even if both the physical and virtual sensors were within the spotlight beams, the system would be acausal. The information arrives at the location of the virtual sensor before the physical sensor and so cannot be used to accurately estimate the error at the virtual sensor, unless the sound field is periodic in nature. In which case the acausality is not important.

A moving virtual sensor.

The success of the virtual sensing algorithm relies on the time invariance of the $\boldsymbol{G}_{vu}$, $\boldsymbol{G}_{pu}$ and ***H*** transfer functions. The $\boldsymbol{G}_{pu}$ transfer function can be updated online by the addition of low level white noise to the secondary source output, however as there is no sensor at the virtual sensor location during operation the estimates of $\boldsymbol{G}_{pu}$ and ***H*** cannot be updated.

If the motion is small compared to the wavelength the algorithm can cope with changes in the position of the virtual sensor. However these problems are exacerbated if the secondary field varies significantly with position. This is the case with the audio spotlight as will be shown in the second half of the paper.

Petersen has also shown that control can be achieved at a moving virtual sensor in a duct, (Petersen 2006b). It was shown that by interpolating between several virtual sensor locations, measured *a-priori* performance could be maintained and was equal to that of a physical sensor.

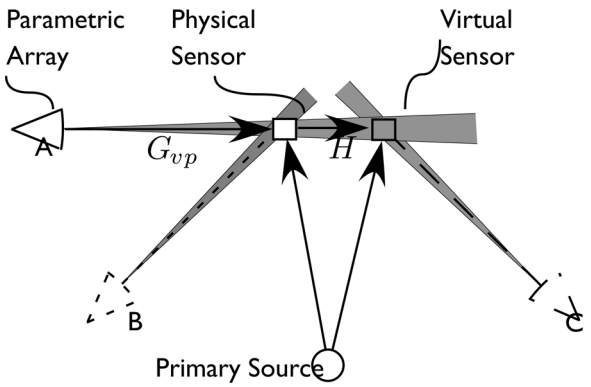

Figure 3 Possible arrangements for the virtual sensor and audio spotlight control system.

THE PARAMETRIC ARRAY

The parametric array first proposed by Westervelt (Westervelt 1963), creates sound due to the non-linear interaction of two sound waves. These carrier waves are ultrasonic in frequency and of a very high level. The mechanism for sound creation is that proposed by Lighthill (Lighthill 1954).

Sound Generation by non-linear interaction

Westervelt showed that Lighthills exact equation for arbitrary fluid motion could be written so that it described the interaction of two sound fields. By neglecting viscous losses and only considering terms up to the second order, the equivalent source strength, *q,* of the iteration can be written as :

$$\Box^2 p_s = -\rho_0 \frac{\partial q}{\partial t} \tag{5}$$

The symbol $\Box^2$ is the De Lambert operator defined as:

$$\Box^2 = \frac{\partial^2}{\partial t^2} - c_0^2 \nabla^2 \tag{6}$$

The source strength q is given by:

$$q = \frac{1}{c_0^4 \rho_0^2}\left[1 + \frac{\rho_0}{2c_0^2}\left(\frac{\partial^2 p}{\partial \rho^2}\right)\Big|_{\rho=\rho_0}\right]\frac{\partial}{\partial t} p_i^2 \tag{7}$$

where c_0, ρ_0 and p are the sound speed, the ambient density and the instantaneous pressure respectively. The pressure amplitude of the source waves is p_i , i=1,2.

Assuming adiabatic behaviour and harmonic signals, the partial differential in equation (6) can be expressed in terms of the ratio of specific heats γ, so that the ratio of q to the source wave pressure amplitude is given as

$$\mathcal{A} = \frac{i(1+\gamma)}{4c_0^4 \rho_0}(\omega_1 \pm \omega_2) p_1 p_2 \tag{8}$$

It can be seen from equation (8) that the strength of the parametric array is proportional to the carrier frequency. For air at standard conditions the first term in equation (8) evaluates to 3×10^{-11}, -210dB.

Berktay (Berktay:1965a) used this model, and showed that if the carrier waves are plane and collimated then the scattered pressure in the far field can be written as equation (9).

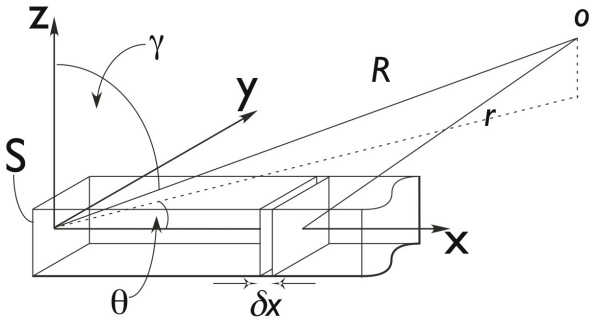

Figure 4 Geometry used by Berktay to solve for the wave scattered by two plane waves interacting.

$$p_s(R,\theta) = \frac{p_1 p_2 \Omega^2 S}{4\pi\rho c^4 R} exp(-\alpha R)\frac{\sin(bk\sin\theta)}{bk\sin\theta} \frac{1}{\sqrt{A^2 + 4k^2\sin^4(\theta/2)}} \tag{9}$$

where S is the area of the beam and b its width in the plane of θ. The absorption at the scattered frequency, Ω is denoted α_s. The angle to the observation point, o, from the axis of the array beam is denoted θ. This angle is assume to be small so that the length of the region of interaction, x, is much less than the distance to the observation point r, i.e. $x << r \rightarrow R \approx r\cos(\theta) + x$.

The length of the interaction zone, x, can be written in terms of the absorption coefficient of the carrier waves α_c. It is assumed that the carrier waves only interact over a finite region that extends to the point where the carrier waves have been significantly attenuated by absorption therefore the length of this virtual source is given by $L = 1/\alpha_c$. For a carrier wave frequency of 50kHz the absorption is $0.23m^{-1}$, (Bass 1995) therefore the source length is 4.35m, (the absorption coefficient was calculated using equations given by Bass *et. al* (Bass 1995)).

The source strength is also proportional to the second derivative of the pressure to the ambient density, $q \propto d^2p/d\rho^2|_{\rho=\rho_0}$. This is a function of the ratio of specific heats. If adiabatic compression is assumed $d^2p/d\rho^2|_{\rho=\rho_0} = (\gamma\text{-}1)c_0^2/\rho_0$. It can be seen that the ratio decreases with frequency, implying the parametric array becomes more efficient at higher frequencies. If the scattered wave is in the audio frequency range the difference in level between the carrier and scattered wave is of the order of 80dB.

Close to the source the majority of the energy is at the source frequencies of 50kHz and 50.1kHz. As the range is increased part of this energy is transferred to the difference frequency, (1kHz). These spectrums were formed from time domain data calculated by a numerical simulation of the non-linear interaction. This numerical model is described in the next section.

The KZK equation

The equation derived by Berktay (Berktay 1965a) is only an approximation and only applies in the far-field. Which for the frequencies we are considering is of the order of 5m. A more accurate method of predicting the sound field created by the parametric array is required. The KZK, (Khokhlov-Zabolotskaya-Kuznetsov) equation models the non-linear response of a fluid at all ranges. The model includes the effects of relaxation phenomena, thermo-viscosity and non-linearity. The numerical algorithm used was developed by

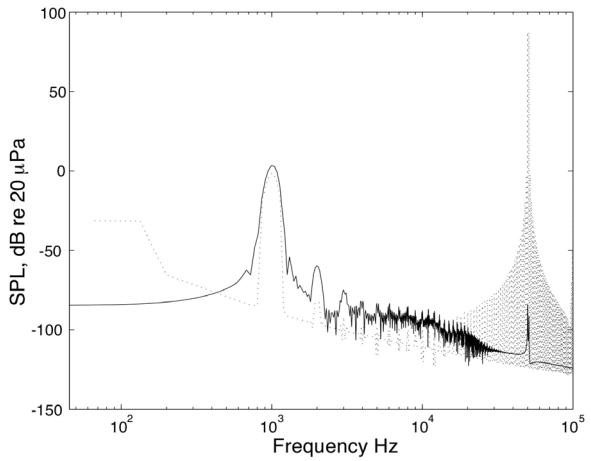

Figure 5 The spectrum of the pressure at z=0.02m, (dashed line), and z = 3.02m, (solid line).

Lee (Lee 1993) and augmented by Cleveland (Cleveland 1996). The algorithm is time domain based.

The KZK equation is

$$\frac{\partial^2 p}{\partial z \partial t'} = \frac{c_0}{2}\left(\frac{\partial^2 p}{\partial r^2} + \frac{1}{r}\frac{\partial p}{\partial r}\right) + \frac{D}{2c_0^3}\frac{\partial^3 p}{\partial t'^3} + \frac{\beta}{2\rho_0 c_0^2}\frac{\partial^2 p}{\partial t'^2} \quad (10)$$

where $t' = t - z/c_0$, the retarded time. $D = \rho_0^{-1}[(\zeta + 4\eta/3) + \kappa(1/c_v + 1/c_p)]$ is the diffusivity of the medium, β is the non-linear coefficient and z is the distance from the source.

This was solved numerically using a program written by Lee and Cleveland (Lee 1993) (Cleveland 1996a).

The parameters for the simulation were:

Carrier Wave: $p_0=(\sin(\omega_0 t) + \sin(1.02\omega_0 t))H(t)$, where H(t) is a Hanning window and $\omega_0=100\pi$ krads^{-1}.

Expected difference frequency: $0.02\omega_0=2\pi$ krads^{-1}.

Time step: 0.2µs

Transducer radius: 0.1m

Fluid properties: $\rho=1.2$ kgm^{-1}, $c_0=343$ ms^{-1}.

Non-linear coefficient: 1.0

The transducer radius of 0.1m gives a Rayleigh distance of 4.35m.

The resulting time series was Fourier transformed to obtain values for the control field pressure at a number of locations. An example of the spectrums at 0.02m and 3.02 is shown in figure 7. The variation of the predicted field with distance on axis and with angle is shown in figures 8 and 9. The results were used to predict the zone of quiet produced when the parametric array is used as a control source. This is discussed in the next section.

EXAMPLE OF ACTIVE CONTROL

In this section the results of active control of a monopole sound field at 1 kHz using the parametric array to create the secondary field are shown. The controlled fields created by a baffled piston as the secondary source and that created by the parametric array are compared. In both scenarios the primary field is generated by a monopole at the origin. The secondary sources are also located at the origin.

The primary field

For this example a simple monopole is assumed as the primary source and the field is governed by the free field Greens function:

$$P(r) = P_0 \frac{e^{jkr}}{r} \quad (11)$$

The amplitude of P_0 is such that P(r)=94dB at 1m. The primary and secondary sources are collocated. This arrangement highlights the difference in the source characteristics of the audio-spotlight and a simple monopole.

The control field

Figure 8 shows the variation in pressure for a monopole and the audio spotlight. The magnitude of the spotlight array has been set so as to equal the monopole field at 5m, (the active control location). The two vertical lines show once and twice the Rayleigh distance. Note that the sound field from the parametric array as only just begun to converge to the free field Greens function at twice the Rayleigh distance. In this case this is approximately 9m. It can be seen from the figure that using the audio spotlight within the Rayleigh distance will lead to higher levels further from the source, as in this range the sound level is still increasing with distance. It should also be noted that conversely the level of the ultrasonic pump waves is still significant within $1/\alpha$ m of the source, where α is the atmospheric absorption at the pump frequency. It can be seen that at 1 meter the pump wave amplitude is 124dB. Howard *et al* discuss the implications of hearing damage from ultrasound in their review paper (Howard 2005). In which they note that the maximum safe levels for ultrasound have been set at 110dB. Although there is a difference in opinion between the American and European Standards bodies.

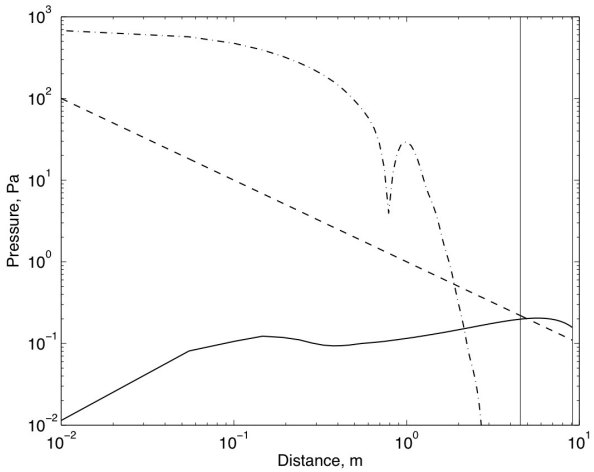

Figure 6 The variation of pressure with distance for a monopole (dashed line) and the audio spotlight, (solid line). The level of the pump wave is shown by the dash-dot line. The two vertical lines indicate once and twice the Rayleigh distance.

The piston field

The zone of quiet was also calculated assuming that the secondary source was a baffled piston of the same radius as the spotlight transducer. The sound field for a piston with unity volume velocity is given by

$$P_{piston}(r,\theta) = \frac{\rho c k}{2\pi r} e^{-jkr}\left[\frac{J_1(ka\sin\theta)}{ka\sin\theta}\right] \quad (12)$$

Figure 9 shows the directivity of the baffled piston and the parametric array. Note that the parametric array pressure was only calculated up to an angle of 3.5 degrees as the computation is very intensive.

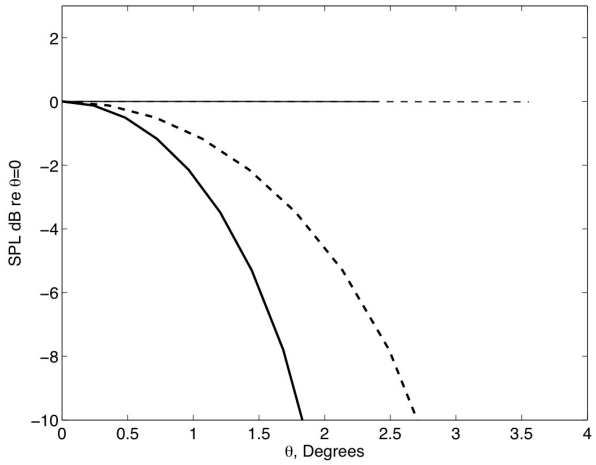

Figure 7 Directivity of the baffled piston (grey lines) and the parametric array (black lines) at 5m (solid line) and 2.5m (dashed line). Note that the angle scale is very small only 0→3.5°.

It can be seen from the figure that the parametric array has a much narrower beam than that of the baffled piston. This results in a smaller area of the controlled sound field being affected by spill over.

Note that the expression used for the sound field of the baffled piston is a far-field expression and so the field close to the piston is not correctly modelled. For this reason the controlled field at distances less than 0.3m should be ignored.

The error sensor

The error sensor is located at 5m. In the following, the control achieved when the secondary source is the parametric array and when it is the baffled piston will be compared. As both the primary and secondary sound fields are known the optimal gain to reduce the combined field to zero at the location of the error sensor can be calculated.

Calculating the optimal control gain

The optimal control gain is simply calculated from the product of the inverse of the secondary path, $\boldsymbol{C}^{-1}$ and the disturbance at the error sensor $\boldsymbol{d}$. In this case only a single error sensor is used and the magnitude of the control gain is not constrained. This means that complete cancellation is expected at the error sensor. This is not a realistic result, however the character of the field around the sensor, *the zone of quiet*, is of interest.

The zone of quiet & comparison to control using a piston as a secondary source

Figure 10 shows the resulting sound field after active control has been applied. The field is normalised to the primary field so that positive numbers indicate an increase in level and negative numbers indicate attenuation. The scale on the figure has been limited to ±10dB to accentuate the variations in level. The calculation of the sound field produced by the parametric array uses coordinates normalised to the radius of the transducer and the Rayliegh distance. For this reason the shape of the sound field shown in figure 10 is a wedge. From Figure 10 it can be seen that the zone of quiet generated by the parametric array is in fact less localised than that created by the baffled piston, however it has a smaller angular extent. The baffled piston creates narrow lines of reduction whereas the parametric array creates a *smudge*. Note that the extent of the predicted field in the *y* direction is only 0.1m at the monopole source location and extends to only 0.3m at 9m from the source in the *z* direction.

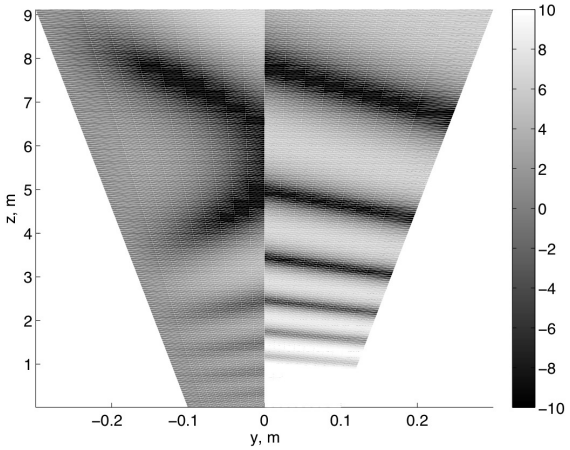

Figure 8 Variation of level of the controlled sound field in space. Left hand plot shows the field created using the parametric array and the right hand plot shows that created using a baffled piston. Note that the scale has been limited to ±10dB to highlight the extent of the zones of quiet.

Figure 11 shows the primary and secondary fields for both the parametric array and the baffled piston. It can be clearly seen that the parametric array creates a very low level close to the source. Figure 12 shows how the controlled field varies on axis. It can be seen that the reduction at the 5m error sensor location is large for both control sources, however the zone extends for a smaller distance for the case of the baffled piston source.

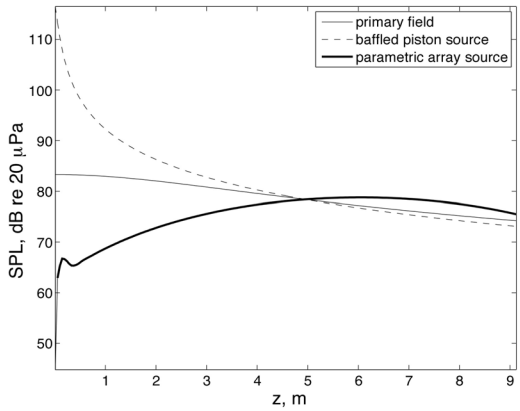

Figure 9 Secondary fields generated by the parametric array and the baffled piston.

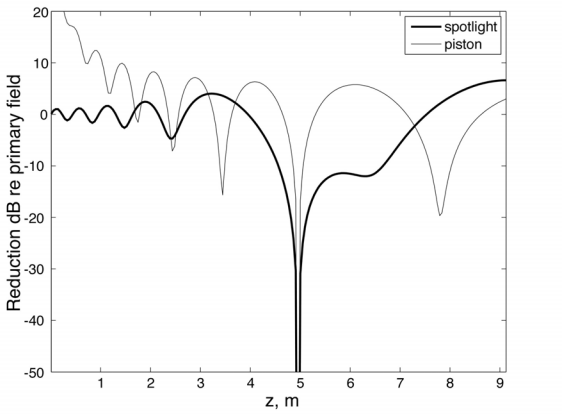

Figure 10 Variation of sound reduction on axis. The black line shows the controlled level due to the parametric array, the grey line shows that due to the baffled piston.

CONCLUSIONS

The virtual sensing algorithm has been reviewed and discussed in the context of creating an active control system that can create mobile, local zones of quiet. It was shown that the algorithm is very sensitive to changes in the transfer functions between the physical and virtual sensors and from the secondary source to the physical and virtual sensors. This would severely limit its application to such a system. The source characteristics of the parametric array have been discussed. It was shown that in the audible range and for medium sized transducers the required ultrasound levels are very high for significant distances on axis and that the audible field does not reach its maximum magnitude for several meters. There is a strong frequency dependence for the efficiency of the source which makes the output of sound below 1kHz impractical.

The parametric array has been shown to create zones of quiet that can extend further in the radial direction over a narrow beam width than those created by a piston. This is a consequence of the degree of geometrical matching between the Greens functions of the sources and the primary field. The use of highly directional sound fields for active control is viable and has some benefits, however the parametric array is not an effective enough transducer. In general the virtual sensing algorithm is not very robust and may be limited to simple sound fields or the virtual location must be fairly close to the physical sensor.

REFERENCES

Bass (1995) Bass, H. E. and Sutherland, L. C. and Zuckerwar, A. J. and Blackstock, D. T. and Hester, D. M. *Atmospheric absorption of sound: Further developments* J. Acoust. Soc. Am, 1995 , 97 , 680-683

Berktay (1965a) Berktay, H. O. Parametric amplification by the use of acoustic non-linearities and some possible applications J. Sound & Vib., 1965 , 2 , 462-470

Cleveland *et al*.(1996) Cleveland, R. O., Hamilton, M. F., Blackstock, D. T., 1996. *Time-domain modelling of finite-amplitude sound in relaxing fluids.* J. Acoust. Soc. Am., 3312--3318.

Cazzolato(2002) Cazzolato, B. S., July 2002. *An adaptive lms virtual microphone.* In: Active 2002. Southampton, UK, pp. 105--116.

Howard (2005) Howard, C.Q., and Hansen C.H., and Zander, A.C. *A Review of Current Ultrasound Exposure Limits* The Journal of Occupational Health and Safety - Australia and New Zealand , 2005 , 21 , 253-257

Kailath (2000) Kailath, T. and Sayed, A. H. and , B Hassibi *Linear Estimation* Prentice Hall, 2000

Kestell, (2000), Kestell, C. D.,Hansen, C. H., Cazzolato, B. S., 2000. *Active noise control in a free field with virtual error sensors.* J. Acoust. Soc. Am 109 (1), 232--243.

Lighthill (1952) Lighthill, M. J. *On sound generated aerodynamically. I. General theory* Proc. Roy. Soc. A, 1952 , 211 , 564-587

Lee (1993) Lee, Y. S. Numerical solution of the KZK equation for pulse finite amplitude sound beams in thermoviscous fluids University of Texas, Austin, 1993

Munn (2003), Munn, J. M., 2003. *Virtual sensors for active noise control.* Phd, School of Mechanical Engineering, University of Adelaide.

Munn (2002a), Munn, J. M., Cazzolato, B., Hansen, C., Kestell, C. D., July 2002. *Higher order virtual sensing for remote active noise control.* In: Active 02. Southampton, UK, pp. 377--386.

Munn (2002b) Munn, J. M., Cazzolato, B. S., Hansen, C. H., November 2002. *Virtual sensing: Open loop vs adaptive lms.* In: Annual Australian Acoustics Society Conference 2002. pp. 24--33.

Nelson (1993), Nelson P, Elliot S, J. *Active Control of Sound,* 1993, Wiley

Petersen (2006a) Petersen, C. D. and Zander, A. C. and Cazzolato, B. S. and Hansen, C. H. *Limits on active noise control performance at virtual sensors* Active, 2006 Adelaide, Australia.

Popovich (1997), Popovich, S. R., 1997. Active acoustic control in remote regions.

Roure (1999), Roure, A., Albarrazin, A., November 1999. *The remote microphone technique for active noise control.* In: Active '99. Fort Lauderdale, FL, USA, pp.1233--1244.

Westervelt (1963), Westervelt, P. J., April 1963. *Parametric acoustic array.* JASA 35 (4), 535--568.